Molecule-like Photodynamics of $Au_{102}(pMBA)_{44}$ Nanocluster

Satu Mustalahti,[†] Pasi Myllyperkiö,[†] Sami Malola,[‡] Tanja Lahtinen,[†] Kirsi Salorinne,[†] Jaakko Koivisto,[†] Hannu Häkkinen,[†,‡] and Mika Pettersson*[,†]

[†]Department of Chemistry and [‡]Department of Physics, Nanoscience Center, University of Jyväskylä, P.O. Box 35, FI-40014 Jyväskylä, Finland

ABSTRACT Photophysical properties of a water-soluble cluster $Au_{102}(pMBA)_{44}$ (*p*MBA = *para*-mercaptobenzoic acid) are studied by ultrafast time-resolved mid-IR spectroscopy and density functional theory calculations in order to distinguish between molecular and metallic behavior. In the mid-IR transient absorption studies, visible or near-infrared light is used to electronically excite the sample, and the subsequent relaxation is monitored by studying the transient absorption of a vibrational mode in the ligands. Based on these studies, a complete picture of energy relaxation dynamics is obtained: (1) 0.5−1.5 ps electronic relaxation, (2) 6.8 ps vibrational cooling, (3) intersystem crossing from the lowest triplet state to the ground state with a time constant 84 ps, and (4) internal conversion to the ground state with a time constant of ~3.5 ns. A remarkable finding based on this work is that a large cluster containing 102 metal atoms behaves like a small molecule in a striking contrast to a previously studied slightly larger $Au_{144}(SC_2H_4Ph)_{60}$ cluster, which shows relaxation typical for metallic particles. These results therefore establish that the transition between molecular and metallic behavior occurs between Au_{102} and Au_{144} species.

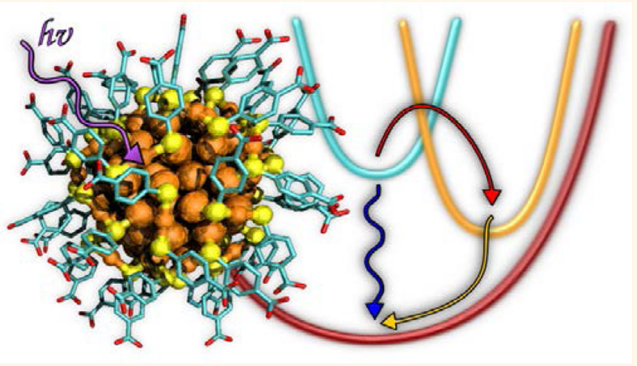

KEYWORDS: gold nanocluster · femtosecond · electronic relaxation · vibrational spectroscopy · transient absorption

Transition from atomic and molecular systems to bulk matter is an important topic for systems at the nanoscale. It is clear that clusters with a few metal atoms are molecule-like, and particles with tens or hundreds of nanometers in size are metal-like.[1,2] The interesting transition region is in the size range of a few nanometers, where the number of metal atoms is close to 100. A key property from the point of view of molecular or metallic behavior is the electronic energy level structure. In particular, the existence or nonexistence of an energy gap or a HOMO−LUMO gap largely dictates the key properties. As long as there is significant gap compared to thermal energy, the system behaves like a molecule: there is electronic stabilization of the structure, and thermal energy is not sufficient to promote electrons to excited states. Excited-state dynamics is described by state-to-state transitions, and radiation is a common phenomenon. When the gap closes, metallic behavior emerges: the electronic state is best described by density and thermal occupation of states; relaxation involves inelastic electron−electron scattering; radiation is very weak; and surface plasmon absorption appears.[1] Optical spectroscopy is well-suited to probe these effects, and when combined with compositionally precise samples, molecular to metallic transition can be studied in great detail.

Monolayer-protected gold clusters are ideal systems for studying transition from molecular to metallic behavior. Recently, it has become possible to synthesize and characterize thiolate-protected gold clusters with a precise composition.[3−7] Absorption spectroscopy has been used for determining the optical gap by locating the onset for electronic absorption.[8−10] It has been found that the $Au_{102}(pMBA)_{44}$ cluster (*p*MBA = *para*-mercaptobenzoic acid) has an optical gap of 0.45 eV,[8] and the $Au_{144}(SC_2H_4Ph)_{60}$ cluster has an optical gap of 0.27 eV.[9,10] However, density functional theory (DFT) calculations showed that Au_{144} does not have an energy gap, and the

* Address correspondence to mika.j.pettersson@jyu.fi.

Received for review November 25, 2014 and accepted February 21, 2015.

Published online February 22, 2015
10.1021/nn506711a

optical gap is higher than the energy gap due to selection rules.[11] Electrochemical experiments are in agreement with this.[12,13] Broadness and weakness of the electronic absorption at the onset is a problem in the determination of the optical gap by absorption spectroscopy. On the other hand, time-resolved measurements are ideally suited for studying the presence of an energy gap, which dramatically affects the lifetime of electronically excited states. Several previous studies have concentrated on small gold clusters, in particular, $Au_{25}(SR)_{18}$ in −1 or neutral charge state and in spherical or elongated shape.[14−19] The main conclusion from these studies has been that a long-lived (>1 ns) electronic excited state exists, implying a molecule-like behavior, which is in agreement with 1.3 eV gap that has been found in absorption and luminescence studies and supported also by DFT calculations.[20−22] Recently, monodisperse samples of $Au_{144}(SR)_{60}$ clusters were studied by transient absorption spectroscopy, and the Au_{144} species was established as a smallest known cluster to exhibit metallic relaxation behavior.[23,24] Earlier studies with less well-defined clusters and nanoparticles proposed a gap opening at ∼300 atoms.[25] Interestingly, as far as we know, between Au_{25} and Au_{144} species, there are no studies of relaxation dynamics of monodisperse samples.

Here, we present results from vis/NIR pump−mid-IR probe studies for $Au_{102}(p\text{MBA})_{44}$ clusters. Our results clearly show that the Au_{102} cluster exhibits molecule-like relaxation behavior with a very long (∼3.5 ns) relaxation time component, establishing that the transition from molecular to metallic relaxation behavior occurs between Au_{102} and Au_{144} species. The photophysics of the cluster can be completely described with a molecular model involving singlet and triplet states, ultrafast intersystem crossing, and internal conversion. A peculiarity of the cluster is that the lowest triplet state relaxes faster than the lowest singlet state due to a smaller energy gap and potential energy surface crossing with the ground state.

RESULTS

The ground-state electronic structure of the $Au_{102}(p\text{MBA})_{44}$ cluster is well-known from our earlier DFT studies.[26] Quantum confinement induces a fundamental HOMO−LUMO and optical gap on the order of 0.5 eV.[8] The electronic states around this gap are composed primarily of Au(6s) states and are ordered into "superatomic" shells in the gold core, signaling a gap closing at 58 free electrons; that is, the manifold of highest occupied states have a 1G shell symmetry, and the lowest unoccupied bands have states of 1H, 2D, and 3S symmetries (Figure 1).[26] These states are also referred to as the Au(6s) free electron states as they would form the continuous free electron conduction band in large colloidal gold particles when the

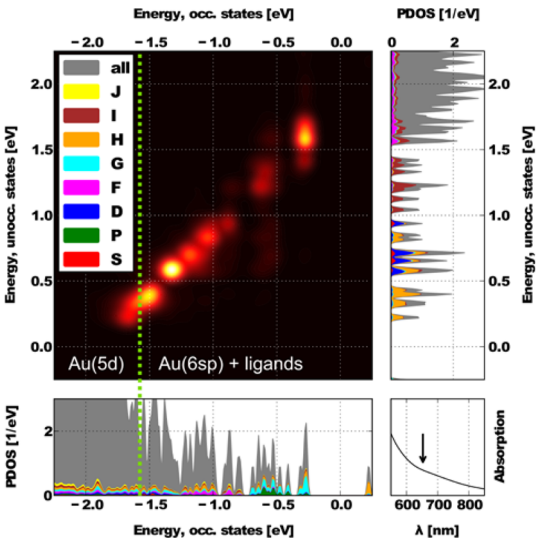

Figure 1. Main panel: transition contribution map analysis of optical transitions at a wavelength of 652 nm (1.9 eV) for the $Au_{102}(p\text{MBA})_{44}$ cluster, as marked by the arrow in the lower right panel. Angular momentum projected electronic density of states is shown for occupied states (horizontal panel) and unoccupied states (vertical panel). The brightness of the yellow area in the correlation plot indicates the contribution from this region of occupied to unoccupied single-electron contribution in the transition. The Fermi energy is at zero. The vertical dashed line denotes the upper edge of the Au(5d) band. In the density of states plot, the individual states are broadened by 0.01 eV Gaussians.

fundamental gap closes at the bulk limit. Sulfur(p)-based ligand states are found below the 1G shell, and the upper edge of the Au(5d) is located at around −1.6 eV, as marked in Figure 1.

We studied the excitation dynamics at the wavelength of 652 nm (1.9 eV). Theoretical analysis by using the time-dependent density functional perturbation theory (for details, see the Methods section) reveals that this excitation involves single-electron states of various character, including intraband Au(6s) → Au(6s) transitions, sulfur(p) → Au(6s) transitions, and interband Au(5d) → Au(6s) transitions (Figure 1). Induced transition density, hole density, and electron density are visualized in real space in Figures S1 and S2 (Supporting Information), and they are localized mostly in the metal core.

A contour plot of the transient absorption spectrum obtained for $Au_{102}(p\text{MBA})_{44}$ at 652 nm excitation is shown in Figure 2. A negative ground-state bleach signal and a positive hot band signal are observed. The bleach signal apparently disappears after ∼20 ps, while the hot band signal shows a decrease in intensity in three different time scales from a fast picosecond component to a long-lived component with a lifetime much longer than our experimental detection window (∼1 ns). Steady-state Fourier transform infrared (FTIR) spectrum of the probed vibration is shown above the contour plot in Figure 2. A representation of the probed vibrational mode is shown in Figure S3 in

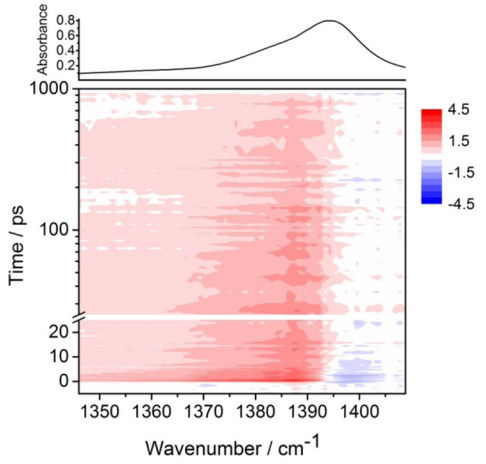

Figure 2. Contour plot of the transient absorption spectrum of the $Au_{102}(pMBA)_{44}$ cluster upon excitation at 652 nm (1.9 eV). The scale of the contour plot is in mOD. Note the logarithmic scale for longer delay times. Steady-state FTIR spectrum of the probed vibration is shown above the contour plot.

Supporting Information. The mode is best described as a mixed C−H bending/C═C stretching.

The data shown in Figure 2 are first analyzed by examining the kinetics of the studied system at different wavenumbers. Four time constants that describe the relaxation processes in the system are obtained by fitting the kinetics at bleach band and hot band maximum. The bleach recovery kinetics could be fitted with a single exponential function convoluted with a Gaussian instrument response function, resulting in a time constant of 6.8 ps. To fit the hot band kinetics, a sum of three exponential functions convoluted with an instrument response function was used. The time constants obtained for hot band relaxation were 1.5 ps, 84 ps, and ∼3.5 ns. The fitted kinetics for hot band and bleach are shown in Figure 3. The excitation fluence dependence of the signal amplitude was observed to be linear, and no pulse energy dependence was found for the time constants. This observation indicates single-photon processes and is compatible with molecular behavior.

Transient absorption spectra were also obtained for two NIR excitation wavelengths at 1304 and 1518 nm. The kinetics for NIR excitations were analyzed similarly to the visible excitation kinetics. The results for hot band and bleach kinetics are shown in Figure 3. While the two longer time constants and bleach disappearance kinetics remained the same for different excitations, the shortest time constant was observed to be shorter for NIR excitation: 600 fs for 1304 nm excitation and 500 fs for 1518 nm excitation. The obtained time constants and their relative amplitudes are summarized in Table 1. When changing from visible to NIR excitation, the amplitude of the fastest component decreases relative to the other components. The amplitude of the shortest component is ∼55% of the

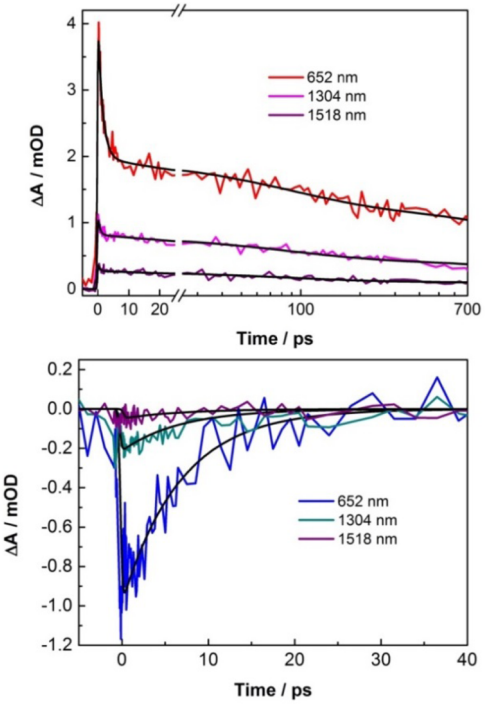

Figure 3. Hot band (top panel) and bleach signal (bottom panel) kinetics obtained with different excitation wavelengths. Exponential fits to the data are shown with black lines.

TABLE 1. Summary of the Time Constants and Relative Amplitudes of Different Hot Band Components for Different Excitation Wavelengths

excitation wavelength	τ_1	τ_2	τ_3	τ_4
652 nm	1.5 ps	84 ps	∼3.5 ns	6.8 ps
	55.3%	16.1%	28.6%	
1304 nm	600 fs	84 ps	∼3.5 ns	6.8 ps
	35.3%	28.7%	36.0%	
1518 nm	500 fs	84 ps	∼3.5 ns	6.8 ps
	40.2%	33.2%	26.5%	

total signal amplitude for 652 nm but decreases to 35−40% for NIR excitation. This change in amplitude ratios is clearly visible in the kinetics shown in the top panel in Figure 3.

In order to more carefully analyze the spectral changes, the transient spectra obtained for visible excitation at several time delays were analyzed by spectral fitting. The measured transient absorption spectra (dotted lines) and obtained fits (solid lines) for a few time delays are shown in Figure 4. The center position and shape for the bleach component were obtained from the fitted steady-state spectrum shown in Figure 2 and were fixed during the spectral fit. The hot band was fitted with two spectral components that have the same overall shape as the bleach component; that is, both components consist of two Gaussians. An example of the fitted components is shown in Figure S4 (Supporting Information). The time evolution of the bleach component amplitude was further studied by

fitting a sum of exponential functions to the amplitudes obtained from the fits for different time delays. This procedure reveals amplitude changes that are hidden behind overlapping bleach and positive components. This can be seen clearly in the time evolution of the amplitude of the bleach component, which is shown in Figure S5 (Supporting Information). The bleach component shows recovery components in intermediate (84 ps) and long (~3.5 ns) time scales, which are not evident in the raw data (see Figures 2–4).

The energies of electronic states of $Au_{102}(SH)_{44}$ in singlet and triplet manifolds were obtained from the DFT calculations. The energies of the lowest singlet and triplet states are shown in Figure 5. Energies of the first excited singlet state and the triplet state were calculated in the ground singlet-state configuration. Additionally, the triplet-state geometry was relaxed, and the energies of different states were calculated in this geometry. The results indicate that there is a structural change in the atomic configuration of the cluster core associated with the change in electronic spin state.

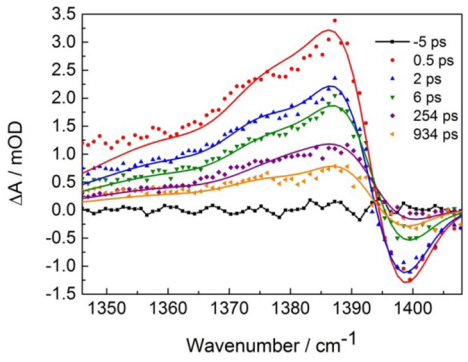

Figure 4. Transient spectra of the $Au_{102}(pMBA)_{44}$ cluster at various time delays. The experimental data are shown by points, and the fits to the data are shown by solid lines.

The changes include rotation-like motion of some of the gold atoms and a slight bulging at the equatorial plane perpendicular to the C_5 axis of the core. These changes are visualized in Figure S6 (Supporting Information). Results for singlet-state energy at relaxed triplet geometry and triplet state in relaxed singlet geometry are shown as dotted lines in Figure 5.

DISCUSSION

From the data presented in Figures 2–5, a complete description of photodynamics for $Au_{102}(pMBA)_{44}$ can be deduced. A summary of the energetics and dynamics is shown in Figure 5. In the following, we interpret the findings and discuss the assignment of different time constants to different relaxation processes.

In order to relate observations to molecular or metallic behavior, we first discuss generally the dynamic properties of these systems. In molecular systems, the photophysics are characterized by single-electron excitation followed by electronic relaxation *via* internal conversion (IC) and intersystem crossing (ISC), vibrational relaxation, and long-lived lowest electronic excited states. Characteristic time scales for relaxation include sub-picosecond for highly excited electronic states, picosecond for vibrational relaxation, nanosecond to microsecond for lowest spin-allowed excited states, and up to seconds or even minutes for lowest spin-forbidden electronic excited states.[27] Due to the long-lived states which originate from large energy gaps, radiation is a common relaxation mechanism. For metallic particles, electronic relaxation is ultrafast and occurs on a time scale of about a picosecond all the way to the electronic ground state, eliminating radiation as a significant relaxation channel. Electronic relaxation is accompanied by excitation of phonons heating up the system thermally. It should be noted, however, that in molecules a similar process

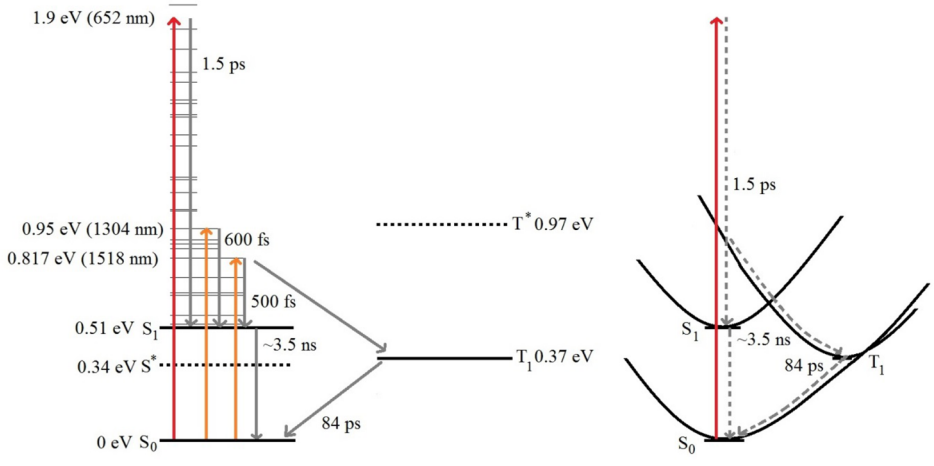

Figure 5. Calculated electronic energy states of $Au_{102}(SH)_{44}$ and the time constants for different relaxation processes. The visible excitation is shown in red, and the NIR excitations are shown in orange. The relaxation is indicated with gray arrows. T* is the triplet state in the relaxed singlet-state geometry, and S* is the singlet (ground) state in the relaxed triplet-state geometry. The thin solid lines show the higher excited states in the singlet manifold.

occurs. Characteristic heat dissipation time is on the order of 10 ps.[1] A major difference of molecular systems is that strong electron−electron scattering equilibrates electron distribution, rapidly converting single-electron excitation to a hot electron distribution, which then equilibrates with lattice phonons by electron−phonon scattering and finally further relaxes toward ambient temperature by heat dissipation to the environment. The fundamental reason for this difference in electronic relaxation between molecular and metallic systems is that, in metallic systems, due to the absence of an energy gap, electrons can accept small amounts of energy from an excited electron *via* collisions, whereas in molecules, this channel is not possible. The transition from molecular to metallic behavior is expected to occur in a quite abrupt manner when the energy gap closes.

Relaxation Dynamics. The most important single observation concerning the molecular behavior is the long-lived (∼3.5 ns) relaxation component of the hot band, which indicates undoubtedly that the $Au_{102}(p\text{MBA})_{44}$ cluster has a significant energy gap. This observation is in agreement with earlier absorption measurements and DFT calculations that yielded an energy gap of 0.45 eV.[8] It should be noted that it is not obvious that an energy gap of 0.45 eV would lead to a long-lived electronic state. The ligands contain carboxylic groups which have O−H stretching vibrations with vibrational frequencies corresponding to the gap energy,[8] offering a channel for fast dissipation of electronic energy to vibrations. Since fast relaxation is not observed, the results indicate that the lowest electronic excited states are not strongly coupled to the ligand vibrations. Thus, the electronic energy relaxes presumably *via* coupling to cluster core phonons and possibly gold−ligand interface vibrations. The frequencies of these modes are very low, corresponding to energies on the order of 10−20 meV,[28] requiring a very high-order phonon process. This explains the long lifetime of the lowest electronic excited states, which also implies that the longest-lived excited electronic state is localized in the cluster core. This is in agreement with the superatom model, which shows localization of the first excited singlet state in the cluster core.[26] The presence of a long-lived state for Au_{102} species shows a striking contrast to the dynamics of the Au_{144} cluster, which relaxes to the ground state with a longest vibrational cooling time constant of ∼20−30 ps,[23,24] in agreement with the energy gap closing deduced for the Au_{144} cluster.[11−13] The difference in relaxation dynamics between the Au_{102} and Au_{144}[24] species is illustrated in Figure S7 (Supporting Information) by comparing the mid-IR transient absorption spectra of the clusters obtained with 652 nm excitation.

Next, we consider the fastest time constant (0.5−1.5 ps), which can be assigned to electronic relaxation of the initially excited state. This relaxation time constant is similar to those previously obtained for the Au_{144} cluster at ∼1[23] and 1.5 ps.[24] The fast relaxation is also compatible with high density of electronic states,[8] which allows energy dissipation *via* one-phonon processes. It should be noted that this process may involve multiple IC as well as ISC processes due to the large spin−orbit coupling of heavy gold atoms. Ultrafast ISC is common in organometallic compounds involving heavy atoms.[29] Electronic relaxation possibly involving ISC has also been observed for the $Au_{25}L_{18}$ cluster that shows charge-state-dependent relaxation dynamics.[19] Since the DFT calculations show that equilibrium geometries of singlet and triplet states are markedly different, it is expected that there are numerous potential energy curve crossings at high excitation energy, allowing fast ISC. This presumably leads to mixed distribution of singlet and triplet states during relaxation.

To elaborate on longer time constants, we inspect Figure 5 in more detail. The singlet−singlet (S_1-S_0) energy gap is 0.51 eV (0.45 eV experimentally), and since the spin states are the same, we do not expect curve crossings between them. This is in contrast to the triplet state and the ground state, which cross close to the equilibrium structure of the triplet state (see Figure 5). Thus, we assign the longest relaxation component at ∼3.5 ns to relaxation of the lowest excited singlet state to the ground state, that is, to IC (S_1-S_0). Since the T_1 is 0.46 eV above the S_1 at the singlet equilibrium geometry, ISC from S_1 to T_1 involves activation energy and occurs efficiently only during electronic relaxation when the system is hot. After being cooled to the bottom of the first excited singlet state, the singlet population is trapped, although the triplet state is lower in energy. On the other hand, curve crossing between T_1 and S_0 provides a channel for fast ISC to the ground state. Thus, the intermediate relaxation time constant (84 ps) is assigned to ISC from the lowest triplet state to the ground state. This situation is uncommon; however, it is readily explained by the relatively small energy gap, significant S_1-T_1 splitting of 0.14 eV, and structural relaxation between singlet and triplet states providing curve crossing. On this basis, we make a prediction that for some larger clusters the triplet, or possibly a higher, spin state may become the ground state, thus making them magnetic.

There is still one observed time constant of 6.8 ps that needs explanation. This is a natural time scale for vibrational relaxation and cooling,[24,30] and we assign it accordingly. Now, we are ready to construct a full picture of the relaxation sequence. Initial excitation accesses a high-energy singlet state which then relaxes in sub-picosecond to picosecond time scales to various electronic states *via* multiple IC and ISC processes, which is facilitated by vibrational motion induced by

simultaneous vibrational heating of the cluster. Part of the singlet population relaxes all the way to the ground state (possibly *via* ISC as an intermediate process), which is clearly seen in the bleach recovery with a time constant of 6.8 ps (see Figure 3). Note that there is no shortest (0.5−1.5 ps) time component in the bleach recovery, which is understandable because the lower limit to the recovery time is determined by the vibrational cooling time on the ground electronic state. When the hot cluster reaches energetically the crossing point of the S_1 and T_1 states, singlet and triplet populations become trapped in their respective potential wells and, finally, relax to the ground state with characteristic time constants.

Next, we consider the effects of changing the excitation wavelength. When excited with longer wavelengths, the relative amplitude and the time constant of the shortest time component decrease compared to excitation with 652 nm (see Figure 3). This dependence can be explained by identifying the amplitude loss with population transfer to the ground electronic state. The factors that determine the kinetics of this process are initial excess energy and cooling rate. As long as the cluster possesses enough energy to reach a crossing point for relaxation, population leaks to the ground state. In this interpretation, the observed time constant is not associated with a single process but reflects the time that the system spends in the energetic window allowing population relaxation to the ground state. With the 652 nm excitation, more excess energy is deposited compared to the NIR excitations, which results in longer time spent with enough energy for relaxing to the ground state. This explains the longer time constant and larger amplitude loss observed for 652 nm excitation compared to NIR excitations. The relaxation to the ground state populates very highly excited vibrational states of the ground electronic state, leading to a significant broadening of the probed vibration. This appears as a fast decay of the amplitude of the transient absorption. This interpretation also gets support from the dynamics studies of the Au_{144} cluster that showed an electronic relaxation time constant of ∼1−1.5 ps for relaxation from highly excited electronic states to the ground state.[23,24]

Spectroscopy of Excited States. Due to the fast vibrational relaxation, the transient spectra past ∼50 ps represent vibrationally cooled spectra of electronic excited states. The spectrum of the singlet state is thus obtained straightforwardly from the spectral fit for the long time asymptote, yielding a shift of ∼4 cm^{-1} from the ground state. Additionally, the intensity of the positive absorption is higher than the ground-state absorption. The spectral shape is practically unchanged after the first ∼10 ps, which means that the spectrum of the triplet state is indistinguishable from the singlet state. It is surprising that such a shift can be observed in the ligand vibration that is localized on the benzene ring. As discussed above, the slow relaxation indicates that the excited electronic states are not significantly coupled to the ligand vibrations, which is in contradiction with the observed vibrational shift. The shift can be explained when taking into account that there is significant structural rearrangement in the cluster core associated with singlet−triplet transition, as indicated by DFT calculations. Such a structural change may induce structural rearrangement in the ligand layer *via* metal−ligand interface coupling. Change of structure may then induce vibrational shifts in the benzene ring vibrations since they are very sensitive to weak interactions with neighboring molecules. The larger intensity of the excited-state absorption can be explained by the same effect. This mechanism bears some similarity with protein dynamics, where a change in a small chromophore molecule triggers a collective structural change in a whole protein structure.

Radiative Relaxation. Since the lowest excited singlet state is long-lived, the question of possible fluorescence arises. In order to estimate the quantum yield (QY) of fluorescence, we assume that the lifetime of the singlet state is 3.5 ns. We obtained the combined oscillator strength of the six lowest excited singlet states that lie within 0.1 eV energy range from DFT calculations as ∼0.001. Using the relation between oscillator strength (f) and radiative rate constant (A_{fi}), $A_{fi} = 2\pi\nu_{fi}e^2f/\varepsilon_0c^3m_e$ yields a radiative lifetime of 1.1×10^{-4} s. This would imply a fluorescence QY of 3×10^{-5}. Thus, we conclude that fluorescence QY for $Au_{102}(p\text{MBA})_{44}$ is small but measurable. Whetten's group has determined the QY for the Au_{28} and Au_{145} clusters as $(3.5 \pm 1.0) \times 10^{-3}$ and $(4.4 \pm 1.5) \times 10^{-5}$, respectively.[20,31] These values are in line with the present estimation for the Au_{102} species. It is interesting that two emission bands were observed for the Au_{28} species with a splitting of 0.35 eV, and a possible interpretation based on singlet and triplet emission was given.[20] The calculated S−T splitting of 0.14 eV for the $Au_{102}(p\text{MBA})_{44}$ supports this interpretation as it is expected that the splitting should be larger for the smaller cluster due to more confined electronic wave function, which yields a larger effect of electron correlation.

CONCLUSIONS

Photodynamics of the $Au_{102}(p\text{MBA})_{44}$ cluster was measured by a vis/NIR pump−mid-IR probe transient absorption method. Aided by results from DFT calculations, we obtained a complete description of relaxation pathways. The cluster relaxes in several time scales: (1) 0.5−1.5 ps electronic relaxation to the ground state, (2) 6.8 ps vibrational cooling, (3) 84 ps ISC from the lowest triplet state to the ground state, and (4) ∼3.5 ns IC from the lowest excited singlet state to the ground

state. The anomalous faster relaxation of the triplet state compared to that of the singlet state is due to the presence of S_0-T_1 curve crossing. Singlet–triplet splitting is 0.14 eV according to DFT calculations. The results show that photodynamics of $Au_{102}(pMBA)_{44}$ can be described with a conventional photophysical model of molecules, establishing that the transition from molecule-like to metallic behavior occurs between Au_{102} and Au_{144} clusters. Vibrational spectra of excited states suggest that there is structural rearrangement of the ligand layer in the excited states driven by photoinduced rearrangement of the cluster core, in analogy to protein dynamics in biological systems. The mid-IR fluorescence quantum yield of the cluster is estimated to be on the order of 10^{-5}. It is predicted that, due to singlet–triplet splitting, some larger clusters may exhibit high-spin ground states when the HOMO–LUMO gap gets very small.

METHODS

Synthesis and Characterization. $Au_{102}(pMBA)_{44}$ clusters were prepared, and a full structural characterization was done as previously published.[32] In order to ensure the monodispersity of the $Au_{102}(pMBA)_{44}$ sample used in this work, a comparison to an earlier batch of $Au_{102}(pMBA)_{44}$ clusters used in the optical absorption studies[8] was made (see Figure S8 in Supporting Information). For the experiments, Na^+ was used as the counterion for deprotonated clusters, and the sample was dissolved in D_2O (99.9% atom D, Aldrich).

Spectroscopic Methods. The FTIR spectrum of the sample was measured with a Nicolet Magna-IR 760 FTIR spectrometer with 1 cm^{-1} spectral resolution. Transient absorption experiments were performed by using an experimental setup similar to that used for the Au_{144} species. The experimental details are described in more detail in ref 24. Three different excitation wavelengths in the vis/NIR region (652, 1304, and 1518 nm) were used in the experiments. The excitation fluence dependence on the system kinetics was determined by using pulse energies between ~50 and 300 nJ for 652 nm excitation.

Computational Methods. We used DFT as implemented in the code package GPAW.[33] GPAW uses projector-augmented waves (PAW) and real-space grids and has scalar-relativistic corrections included in the Au atom setup. We used both the full and reduced Au_{102} cluster models. The full model included the *p*MBA ligand layer, and it was relaxed to a theoretical optimal structure starting from the published crystal structure (ref 3) and using 0.2 Å grid spacing and Perdew–Burke–Ernzerhof (PBE) functional. Optical absorption spectrum of the full $Au_{102}(pMBA)_{44}$ was evaluated from the linear response time-dependent DFT formalism (ref 34) by using the PBE functional in the exchange-correlation kernel. The characteristics of the excitations at 652 nm (1.9 eV) were analyzed by using a method that some of us published recently.[35] Based on the time-dependent DFT perturbation theory, we evaluated the so-called transition contribution map, the real-space transition density, and contributions from hole and electron densities. Magnetic states were calculated by using LDA functional and the reduced Au_{102} model, where the *p*MBA ligands were replaced by SH groups, preserving the same overall electronic structure in the metal core. The atomic structure was rerelaxed for every fixed spin configuration separately. We also checked the relative total energies of spin configurations by using the PBE functional, which did not affect the overall conclusions. Energies of the clusters were reported relative to the energy of the relaxed singlet-state configuration, which is the lowest energy state of all calculated configurations. The first excited states of singlets and triplets were estimated directly based on the HOMO–LUMO gap separately for each spin configuration in question.

Conflict of Interest: The authors declare no competing financial interest.

Supporting Information Available: Excitation induced transition density (S1), electron and hole densities (S2), representation of the probed vibrational mode of the *p*MBA ligand (S3), an example on spectral fitting (S4 and S5), computational results of spin-state-associated changes in the gold core configuration (S6), comparison of the transient absorption spectrum of the $Au_{102}(pMBA)_{44}$ cluster to the one measured previously for $Au_{144}(SCH_2CH_2Ph)_{60}$ (S7), and further analysis on the monodisperse nature of Au_{102} sample (S8). This material is available free of charge *via* the Internet at http://pubs.acs.org.

Acknowledgment. This work was supported by the Academy of Finland and the NGS-NANO and LASKEMO graduate schools. Computational resources were provided by the CSC in Espoo, Finland, and HLRS-GAUSS center in Stuttgart, Germany, through the EU PRACE infrastructure.

REFERENCES AND NOTES

1. Hartland, G. Optical Studies of Dynamics in Noble Metal Nanostructures. *Chem. Rev.* **2011**, *111*, 3858–3887.
2. Qian, H.; Zhu, M.; Wu, Z.; Jin, R. Quantum Sized Gold Nanoclusters with Atomic Precision. *Acc. Chem. Res.* **2012**, *45*, 1470–1479.
3. Jadzinsky, P. D.; Calero, G.; Ackerson, C. J.; Bushnell, D. A.; Kornberg, R. D. Structure of a Thiol Monolayer-Protected Gold Nanoparticle at 1.1 Å Resolution. *Science* **2007**, *318*, 430–433.
4. Heaven, M. W.; Dass, A.; White, P. S.; Holt, K. M.; Murray, R. W. Crystal Structure of the Gold Nanoparticle $[N(C_8H_{17})_4]^-[Au_{25}(SCH_2CH_2Ph)_{18}]$. *J. Am. Chem. Soc.* **2008**, *130*, 3754–3755.
5. Zeng, C.; Li, T.; Dass, A.; Rosi, N. L.; Jin, R. Chiral Structure of Thiolate-Protected 28-Gold-Atom Nanocluster Determined by X-ray Crystallography. *J. Am. Chem. Soc.* **2013**, *135*, 10011–10013.
6. Zeng, C.; Qian, H.; Li, T.; Li, G.; Rosi, N. L.; Yoon, B.; Barnett, R. N.; Whetten, R. L.; Landman, U.; Jin, R. Total Structure and Electronic Properties of the Gold Nanocrystal $Au_{36}(SR)_{24}$. *Angew. Chem., Int. Ed.* **2012**, *51*, 13114–13118.
7. Qian, H.; Eckenhoff, W. T.; Zhu, Y.; Pintauer, T.; Jin, R. Total Structure Determination of Thiolate-Protected Au_{38} Nanoparticles. *J. Am. Chem. Soc.* **2010**, *132*, 8280–8281.
8. Hulkko, E.; Lopez-Acevedo, O.; Koivisto, J.; Levi-Kalisman, Y.; Kornberg, R. D.; Pettersson, M.; Häkkinen, H. Electronic and Vibrational Signatures of the $Au_{102}(p\text{-}MBA)_{44}$ Cluster. *J. Am. Chem. Soc.* **2011**, *133*, 3752–3755.
9. Koivisto, J.; Malola, S.; Kumara, C.; Dass, A.; Häkkinen, H.; Pettersson, M. Experimental and Theoretical Determination of the Optical Gap of the $Au_{144}(SC_2H_4Ph)_{60}$ Cluster and the $(Au/Ag)_{144}(SC_2H_4Ph)_{60}$ Nanoalloys. *J. Phys. Chem. Lett.* **2012**, *3*, 3076–3080.
10. Koivisto, J.; Salorinne, K.; Mustalahti, S.; Lahtinen, T.; Malola, S.; Häkkinen, H.; Pettersson, M. Vibrational Perturbations and Ligand–Layer Coupling in a Single Crystal of $Au_{144}(SC_2H_4Ph)_{60}$ Nanocluster. *J. Phys. Chem. Lett.* **2014**, *5*, 387–392.
11. Lopez-Acevedo, O.; Akola, J.; Whetten, R. L.; Grönbeck, H.; Häkkinen, H. Structure and Bonding in the Ubiquitous Icosahedral Metallic Gold Cluster $Au_{144}(SR)_{60}$. *J. Phys. Chem. C* **2009**, *113*, 5035–5038.
12. Hicks, J. F.; Miles, D. T.; Murray, R. W. Quantized Double-Layer Charging of Highly Monodisperse Metal Nanoparticles. *J. Am. Chem. Soc.* **2002**, *124*, 13322–13328.
13. Quinn, B. M.; Liljeroth, P.; Ruiz, V.; Laaksonen, T.; Kontturi, K. Electrochemical Resolution of 15 Oxidation States for

Monolayer Protected Gold Nanoparticles. *J. Am. Chem. Soc.* **2003**, *125*, 6644–6645.
14. Smith, B. A.; Zhang, J. Z.; Giebel, U.; Schmid, G. Direct Probe of Size-Dependent Electronic Relaxation in Single-Sized Au and Nearly Monodisperse Pt Colloidal Nano-particles. *Chem. Phys. Lett.* **1997**, *270*, 139–144.
15. Link, S.; El-Sayed, M. A.; Schaaff, T. G.; Whetten, R. L. Transition from Nanoparticle to Molecular Behavior: A Femtosecond Transient Absorption Study of a Size-Selected 28 Atom Gold Cluster. *Chem. Phys. Lett.* **2002**, *356*, 240–246.
16. Miller, S. A.; Womick, J. M.; Parker, J. F.; Murray, R. W.; Moran, A. M. Femtosecond Relaxation Dynamics of $Au_{25}L_{18}^-$ Monolayer-Protected Clusters. *J. Phys. Chem. C* **2009**, *113*, 9440–9444.
17. Qian, H.; Sfeir, M. Y.; Jin, R. Ultrafast Dynamics of $[Au_{25}(SR)_{18}]^q$ Nanoclusters: Effects of Charge State. *J. Phys. Chem. C* **2010**, *114*, 19935–19940.
18. Sfeir, M. Y.; Qian, H.; Nobusada, K.; Jin, R. Ultrafast Relaxation Dynamics of Rod-Shaped 25-Atom Gold Nanoclusters. *J. Phys. Chem. C* **2011**, *115*, 6200–6207.
19. Green, T. D.; Knappenberger, K. L. Relaxation Dynamics of $Au_{25}L_{18}$ Nanoclusters Studied by Femtosecond Time-Resolved Near Infrared Transient Absorption Spectroscopy. *Nanoscale* **2012**, *4*, 4111–4118.
20. Link, S.; Beeby, A.; Fitzgerald, S.; El-Sayed, M. A.; Schaaff, T. G.; Whetten, R. L. Visible to Infrared Luminescence from a 28-Atom Gold Cluster. *J. Phys. Chem. B* **2002**, *106*, 3410–3415.
21. Zhu, M.; Aikens, C. M.; Hollander, F. J.; Schatz, G. C.; Jin, R. Correlating the Crystal Structure of a Thiol-Protected Au_{25} Cluster and Optical Properties. *J. Am. Chem. Soc.* **2008**, *130*, 5883–5885.
22. Akola, J.; Walter, M.; Whetten, R. L.; Häkkinen, H.; Grönbeck, H. On the Structure of Thiolate-Protected Au_{25}. *J. Am. Chem. Soc.* **2008**, *130*, 3756–3757.
23. Yi, C.; Tofanelli, M. A.; Ackerson, C. J.; Knappenberger, K. L. Optical Properties and Electronic Energy Relaxation of Metallic $Au_{144}(SR)_{60}$ Nanoclusters. *J. Am. Chem. Soc.* **2013**, *135*, 18222–18228.
24. Mustalahti, S.; Myllyperkiö, P.; Lahtinen, T.; Salorinne, K.; Malola, S.; Koivisto, J.; Häkkinen, H.; Pettersson, M. Ultrafast Electronic Relaxation and Vibrational Cooling Dynamics of $Au_{144}(SC_2H_4Ph)_{60}$ Nanocluster Probed by Transient Mid-IR Spectroscopy. *J. Phys. Chem. C* **2014**, *118*, 18233–18239.
25. Varnavski, O.; Ramakrishna, G.; Kim, J.; Lee, D.; Goodson, T. Critical Size for the Observation of Quantum Confinement in Optically Excited Gold Clusters. *J. Am. Chem. Soc.* **2010**, *132*, 16–17.
26. Walter, M.; Akola, J.; Lopez-Acevedo, O.; Jadzinsky, P. B.; Calero, G.; Ackerson, C. J.; Whetten, R. L.; Grönbeck, H.; Häkkinen, H. A Unified View of Ligand-Protected Gold Clusters as Superatom Complexes. *Proc. Natl. Acad. Sci. U. S.A.* **2008**, *105*, 9157–9162.
27. Turro, N. J.; Ramamurthy, V.; Scaiano, J. C. *Principles of Molecular Photochemistry: An Introduction*; University Science Books: Sausalito, CA, 2009.
28. Varnholt, B.; Oulevey, P.; Luber, S.; Kumara, C.; Dass, A.; Burgi, T. Structural Information on the Au−S Interface of Thiolate-Protected Gold Clusters: A Raman Spectroscopy Study. *J. Phys. Chem. C* **2014**, *118*, 9604–9611.
29. Juban, E. A.; McCusker, J. K. Ultrafast Dynamics of ^2E State Formation in $Cr(acac)_3$. *J. Am. Chem. Soc.* **2005**, *127*, 6857–6865.
30. Maçôas, E. M. S.; Kananavicius, R.; Myllyperkiö, P.; Pettersson, M.; Kunttu, H. Relaxation Dynamics of $Cr(acac)_3$ Probed by Ultrafast Infrared Spectroscopy. *J. Am. Chem. Soc.* **2007**, *129*, 8934–8935.
31. Bigioni, T. P.; Whetten, R. L.; Dag, Ö. Near-Infrared Luminescence from Small Gold Nanocrystals. *J. Phys. Chem. B* **2000**, *104*, 6983–6986.
32. Salorinne, K.; Lahtinen, T.; Malola, S.; Koivisto, J.; Häkkinen, H. Solvation Chemistry of Water-Soluble Thiol-Protected Gold Nanocluster Au_{102} from DOSY NMR Spectroscopy and DFT Calculations. *Nanoscale* **2014**, *6*, 7823–7826.
33. Enkovaara, J.; Rostagaard, C.; Mortensen, J. J.; Chen, J.; Dułak, M.; Ferrighi, L.; Gavnholt, J.; Glinsvad, C.; Haikola, V.; Hansen, H. A.; Kristoffersen, H. H.; Kuisma, M.; Larsen, A. H.; Lehtovaara, L.; Ljungberg, M.; Lopez-Acevedo, O.; Moses, P. G.; Ojanen, J.; Olsen, T.; Petzold, V.; Romero, N. A.; Stausholm-Moller, J.; Strange, M.; Tritsaris, G. A.; Vanin, M.; Walter, M.; Hammer, B.; Häkkinen, H.; Madsen, G. K. H.; Nieminen, R. M.; Norskov, J. K.; Puska, M.; Rantala, T. T.; Schiotz, J.; Thygesen, K. S.; Jacobsen, K. W. J. Electronic Structure Calculations with GPAW: A Real-Space Implementation of the Projector Augmented-Wave Method. *J. Phys.: Condens. Matter* **2010**, *22*, 253202.
34. Walter, M.; Häkkinen, H.; Lehtovaara, L.; Puska, M.; Enkovaara, J.; Rostgaard, C.; Mortensen, J. J. Time-Dependent Density-Functional Theory in the Projector Augmented-Wave Method. *J. Chem. Phys.* **2008**, *128*, 244101.
35. Malola, S.; Lehtovaara, L.; Enkovaara, J.; Häkkinen, H. Birth of the Localized Surface Plasmon Resonance in Monolayer-Protected Gold Nanoclusters. *ACS Nano* **2013**, *7*, 10263–10270.